3D DOT Brain Imaging: An Anatomical Atlas-Based Method

Y. Xu[1,2], Y. Pei[2], R.L. Barbour[1,2]

[1]SUNY Downstate Medical Center, Box 25, 450 Clarkson Avenue, Brooklyn, New York 11203
[2]NIRx Medical Technologies LLC, 15 Cherry Lane, Glen Head, NY 11545

Introduction

For functional neuroimaging modalities, a capability that is increasingly regarded as essential is the ability to map image findings to the underlying anatomy. In the case of diffuse optical tomography (DOT), complicating the goal of mapping DOT activation findings to brain anatomy is the need for a representative atlas that can support the flexible generation of the imaging operator for any selected optode arrangement. Whereas access to individual structural maps is increasingly common, efforts to generate individualized finite element method (FEM) meshes in support of DOT reconstructions can be burdensome. To facilitate the accurate generation and mapping of DOT findings, we have established a library of FEM meshes from a selected MRI atlas that has been segmented according to different tissue types. Specification of optode arrangement corresponding to individual or multiple head regions is made either by graphical selection, or through the loading of measures of head-shape and optode position followed by an affine transformation based on measured fiducials. This information is used to configure the corresponding imaging operators obtained from a precalculated database. Experimental evaluation has shown that determination of head shape, optode location, reconstruction of activation maps and mapping to individual atlases can be made with high fidelity.

Methods

MR-based FEM model library: A single-subject MRI of the brain, having a 1 mm resolution and obtained form Source Signal Imaging, was used as our atlas in the present study [1]. The image was segmented into five classes including skin, skull, cerebrospinal fluid, gray matter, and white matter. The FEM model library consists of the FEM meshes of brain regions of interest (ROIs) and corresponding forward solutions to the photon diffusion equation for identified tissues. Each ROI mesh is generated from the segmented image atlas by use of EMSE MR Viewer [1], in which there are nearly 3000 -3500 nodes, as shown in Fig. 1A. The spatial extent of each mesh file normally covers about 50-75 cm2 on the surface of the head and has a depth of up to 5 cm. In order to cover all regions of brain, we have generated 25 overlapping ROI meshes in our library. Fig. 1B shows twelve ROI meshes of the library.

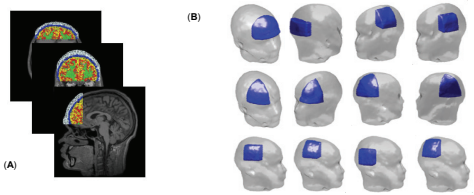

Figure 1. MRI-based segmented FEM brain mesh library.

In each ROI mesh there are about 400 boundary nodes on the surface of the head with approximately a 4 mm spatial resolution. We consider the surface nodes as the possible source/detector positions, and numerically solve the FEM discretized photon diffusion equations using Type III boundary conditions [2]:

$$[A]\{\Phi\} = \{b\}$$
$$[A]\{\partial\Phi/\partial\chi\} = \{\partial b/\partial\chi\} - [\partial A/\partial\chi]\{\Phi\}$$

Solutions to these equations {Φ} and {∂Φ/∂χ} provide the reference detector values and weight functions (Jacobian operators), respectively. The pre-calculated results are incorporated into the FEM model database. The complete brain FEM model database represents over 200 G bytes of data.

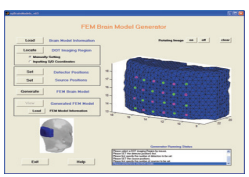

Figure 2. FEM Brain Model Generator.

To efficiently and conveniently employ the model library, we have developed a Matlab-based interactive FEM model generation tool: FEM Brain Model Generator, as shown in Figure 2. By using the generator, the users can easily generate themselves FEM brain models matching the experimental source/detector geometries by inputting the coordinates of source/detector positions and brain fiducial points measured by 3D digitizer, or by using the generator GUI to manually specify source and detector positions on the head surface of the image atlas.

3D Digitizing and registration: Mapping of optode-position information from an individual subject to an FEM library model, is accomplished by first digitizing brain fiducial points and source/detector positions and then applying an affine transformation. The fiducials and optode positions can be measured by a commercial 3D digitizer, e.g., Polhemus patriot, as shown in Figure 3A. Figure 3B illustrates thirteen 10-20 system points that are selected as the standard head shape fiducials in our method. The measured coordinates (P_f) of 13 fiducial points on individual subject head surface and the known coordinates (P_0) of 13 fiducial points on the image atlas surface are related by an affine transformation matrix (M) [3]:

$$P_0 = P_f M$$

Where

$$P_0 = \begin{bmatrix} x_1 & y_1 & z_1 & 1 \\ x_2 & y_2 & z_2 & 1 \\ \vdots & \vdots & \vdots & \vdots \\ x_{13} & y_{13} & z_{13} & 1 \end{bmatrix}, \quad P_f = \begin{bmatrix} x_{f1} & y_{f1} & z_{f1} & 1 \\ x_{f2} & y_{f2} & z_{f2} & 1 \\ \vdots & \vdots & \vdots & \vdots \\ x_{f13} & y_{f13} & z_{f13} & 1 \end{bmatrix}, \quad M = \begin{bmatrix} m_{11} & m_{12} & m_{13} & 0 \\ m_{21} & m_{22} & m_{23} & 0 \\ m_{31} & m_{32} & m_{33} & 0 \\ m_{41} & m_{42} & m_{43} & 1 \end{bmatrix}.$$

From the equation above, the affine transformation matrix M can be solved by a least square method using matrix left division:

$$M = P_f \backslash P_0$$

Next, the measured optode coordinates P_d are registered to the image atlas by following affine transformation:

$$P_i = P_d M$$

where P_i is the registered optode coordinate matrix.

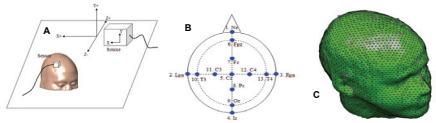

Figure 3. (A) 3D Digitizing; (B) Definition of fiducial points; (C) Image atlas and fiducial points (pink dots).

Anatomical labeling of DOT image: The considered capability has been integrated into our NAVI computing environment [4] to support model-based DOT reconstruction and generation of MR-based montages. Also available are tool boxes that support mapping of the atlas-based reconstructions to other selected atlases (individual, other). Resulting DOT images are compatible with other useful public resources for anatomical analysis. As an extension of our method, we have registered the AAL of SPM (Automated Anatomical Labeling) brain atlas, in which 90 anatomical volumes of interest were reconstructed and assigned a label [5], to our image atlas by an affine transformation, as shown in Figure 4. This allows for the query of registered DOT images so as to identify specific brain regions.

Figure 4. (A) Image atlas; (B) AAL brain atlas; (C) Registration of AAL brain onto image brain.

Results

Qualitative and quantitative assessments of the fidelity of our method are presented here.

3D digitizing and registration: Shown in Figure 5 and Table 1 are experimental results of 3D digitizing and registration for four points on a solid brain phantom. Figure 5(A) shows the comparison of the spatial contours from the phantom (blue) and the corresponding contours from the image atlas (green). Figures 5(B) and 5(C) show the four registered points on the image atlas. Listed in the Table 1 are measures of the precision (CV = ~0.1%) and accuracy (2-5 mm error) of this registration for eight consecutive trials.

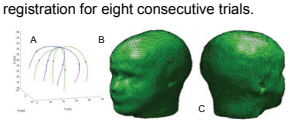

Figure 5. (A) Comparison of the spatial contours: phantom (blue) and image atlas (green); (B) and (C) Registered points on image atlas: ideal (red) and registered (pink).

Measured Point	P1			P2			P3			P4		
	X	Y	Z	X	Y	Z	X	Y	Z	X	Y	Z
Mean	13.89	4.676	20.57	12.64	22.72	19.32	20.83	12.52	18.49	4.791	12.43	18.14
Registered	13.35	4.767	20.74	12.87	22.55	19.68	20.91	12.84	18.27	4.712	12.67	18.00
STD	0.036	0.011	0.030	0.044	0.010	0.031	0.009	0.032	0.053	0.009	0.026	0.041
Distance (1-6 ft)	0.1953			0.4580			0.3928			0.2905		

Table 1. Quantitative results and accuracy of registration.

Sensitivity of 3D Image Mapping to Initial Guess: Table 2 shows AAL mapping results from synthetic data that explore the sensitivity of mapping accuracy on increasing errors in the intial guess. Considered are four target media whose optical properties increasingly differ from intial guess in μ_a only (expect target D). Conditions explored: Optode array 24S x 24D covering 4 x 10 cm area, symmetric to midline. ROI: 1.5 cm object, mean depth 2 cm, middle of occipital cortex. Initial Guess: μ_a=0.06, μ_s=10 cm^{-1}, Target Media (background): A, μ_a=0.06, B, 0.12, C, 0.15 cm^{-1}, ROI, 2x μ_a background; D = B except inhomogenous background (CSF layer, 10% background). Listed values are percentage of total volume contained by indicated tissue types (50% max threshold). Results demonstrate good fidelity to increasing errors in initial guess.

Figure 6 shows position of ROI, Panel A, reconstructed result for target medium A, Panel B. Panel C: affine transformation to representative subject; Panel D, example of representative AAL finding. Findings support accurate mapping of image finding both to fNIRS image atlas and individual MR.

Table 2. Anatomical labels and percentages per cluster in reconstructed inclusion region for four target media

Label	Ideal (%)	Target Medium (error, %)			
		A	B	C	D
Cuneus_L	51	1.96	5.88	7.84	17.6
Calcarine_L	24	0	4.17	4.17	20.8
Cuneus_R	15	6.67	13.3	20.0	13.3
(others)	10	0	20.0	0	20.0

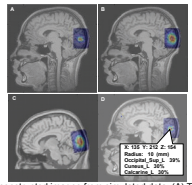

Figure 6. Reconstructed images from simulated data: (A) Target; (B) Reconstructed image; (C) Registered image; (D) Anatomical labeling.

Experimental Validation with Programmable Anthropomorphic Head Phantom: Results in Figure 7 show image overlay obtained from frontal cortex study on head phantom containing programmable electrochormic cell to mimic hemoglobin signal [6]. The 1.2x1.2x0.2 (cm^3) cell is embeded in right frontal brain to a depth of ~2 cm below the head surface. Positionally error of highest contrast pixel is < 3mm. Figure 8 shows result of Fourier Transform for programmed and recovered function.

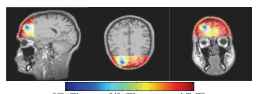

Figure 7. Reconstructed GLM log p-value images from phantom experimental data.

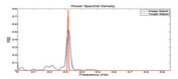

Figure 8. Power spectral density distributions of LC cell driven signal (red) and reconstructed signal (blue).

Recently, some capabilities have been extended to visualize the NIRS data. Examples are presented in Figure 9.

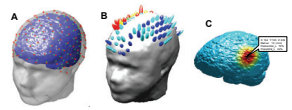

Figure 9. (A) Extended 10-20 system points registered onto the image atlas; (B) Multi-dimensional NIRS data visualization using hyperquadric glyphs; (C) Cortical map and anatomical labeling.

Conclusions

In summary, we have developed an anatomical atlas-based method for efficient generation and registration of 3D DOT image findings. As confirmed by numerical simulations and experimental data from solid-state programmable phantoms, our method is computation-efficient and is able to carry out, with high spatial and temporal accuracies, the necessary mappings—of optode-position information from an individual subject to an FEM library model, and of volumetric image information from the model back to the individual.

References

[1] http://www.sourcesignal.com
[2] K. D. Paulsen and H. Jiang, "Spatially-varying optical property reconstruction using a finite element diffusion equation approximation," *Med. Phys.*, vol. 22, pp. 691–702, 1995.
[3] A. K. Singh, M. Okamoto, et. al., "Spatial registration of multichannel multi-subject fNIRS data to MNI space without MRI," NeuroImage, 27, 842-851, 2005.
[4] Y. Pei, Y. Xu, and R.L. Barbour, "NAVI-SciPort solution: A problem solving environment (PSE) for NIRS data analysis," Poster No. 221 M-AM at Human Brain Mapping 2007 (Chicago, IL, June 10-14, 2007).
[5] N. Tzourio-Mazoyer, B. Landeau, et. al., "Automated Anatomical Labeling og Activations in SPM Using a Macroscopic Anatomical Parcellation of the MNI MRI Single-Subject Brain," NeuroImage, 15, 273-289, 2002.
[6] R.L. Barbour, R. Ansari, R. Al abdi, et. al., "Validation of near infrared spectroscopic (NIRS) imaging using programmable phantoms," *Proceedings of SPIE, Vol. 6870*, R.J. Nordstrom, Ed. (2008).

This work was supported under grant nos. 1R41NS050007-01, 1R42NS050007-02, and 2R44NS049734-02.